Non-Uniform Three-Dimensional Pulsating Heat Pipe for Anti-Gravity High-Flux Applications

Chih-Yung Tseng [1,2,*], **Kai-Shing Yang [3]** and **Chi-Chuan Wang [2]**

[1] Green Energy and Environment Research Laboratories, Industrial Technology Research Institute, 195, Sec. 4, Chung Hsing Rd., Hsinchu 310, Taiwan

[2] Department of Mechanical Engineering, Faculty of Engineering, National Chiao Tung University, EE474, 1001 University Rd., Hsinchu 300, Taiwan; ccwang@mail.nctu.edu.tw

[3] Deparment of Refrigeration, Air Conditioning and Energy Engineering, Faculty of Engineering, National Chin-Yi University of Technology, 51, Sec. 2, Chung-Shan Rd., Taichung 411, Taiwan; ksyang@ncut.edu.tw

[*] Correspondence: chihyungtseng@itri.org.tw; Tel.: +886-3-5917495

Abstract: This study proposes a novel high-flux pulsating heat pipe that can lift the major constraint of the conventional pulsating heat pipe (PHP) which is unable to function properly upon anti-gravity operations. The proposed PHP introduces additional unbalance force via uneven tube diameter/geometry in the adiabatic sections to tailor the problem in anti-gravity operation. The design contains a three-dimensional configuration circuitry with compact arrangement tubes on the evaporator and condenser. Through this design, the non-uniform three-dimensional pulsating heat pipe (3D-PHP) manipulates the uneven inner diameters of the adiabatic sections to form uneven vapor/liquid distributions in the adiabatic sections to yield a unitary flow pattern that is able to withstand a much higher input power. The present PHP uses methanol as working fluid, with 38% volumetric filling ratio, and has a high-flux of 22.9 W/cm^2 and a low the thermal resistance ratio ($R_{\text{anti-gravity}}/R_{\text{gravity-assisted}}$) of 1.05 when the input power is 800 W. Both the heat flux and thermal resistance ratio for the proposed design are far better than the existing literature.

Keywords: pulsating heat pipe; anti-gravity; compact arrangement; thermal resistance ratio

1. Introduction

High-flux electronic devices are dominating the market with the rise of computational power and shrinkage of electronic circuitry. This can be seen almost everywhere, such as with computers, network switches for data centers, laser projectors and high-power LED lighting. To facilitate effective heat transport, the need for high thermal conductivity becomes a must-have as far as effective thermal management is concerned. The mostly used metals like copper or aluminum contain a thermal conductivity in the order of 200–400 W/(mK). To further increase the effective thermal conductivity, the conventional heat pipe that makes use of a two-phase transportation that can raise the equivalent thermal conductivity around 5000 W/(mK) is popularly used in electronic cooling. The maximum heat transfer rate of the heat pipe is mainly limited by the circulation limit of the wick structure. In this regard, typical heat pipes are not suitable for high-flux applications or long-distance transportation.

Unlike conventional heat pipes, the conventional pulsating heat pipe (PHP) is wickless and features long-distance transport capability, yet it can handle multiple heat sources or a heat source with a large area. PHP is bent into a close-loop serpentine shape configuration by a long continuous capillary tube, which consists of several straight pipes and bent tubes, and some working fluid. PHP can be divided into three parts: evaporating section, condensing section and adiabatic section, as shown in Figure 1. With the dimension of the capillary tube, the working fluid in the tubes forms a train of

randomly sized liquid slugs and vapor bubbles because of surface tension. When the evaporating section receives heat to heat up the working fluid and the condensing section dissipations heat to cool down the working fluid, the net pressure difference between the evaporating section and condensing section pushes the liquid slugs and vapor bubbles toward the other section and results in circulation.
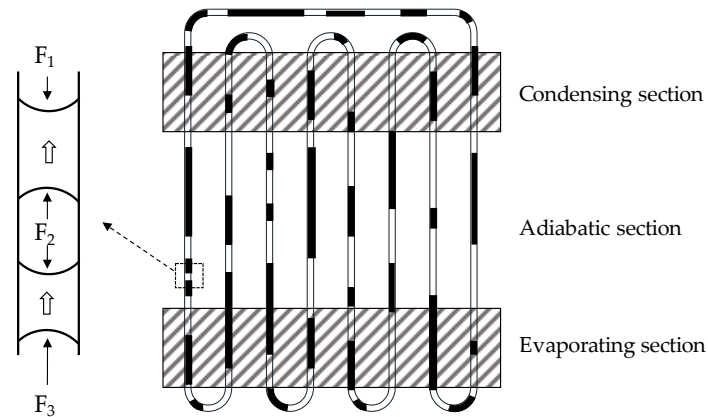

Figure 1. Schematic of a conventional pulsating heat pipe (PHP).

With the working fluid is being randomly distributed, the PHP produces unbalanced flow resistance, so the working fluid has different flow patterns under different heating powers. When the power is lower, the net force can only overcome the flow resistance and transport the vapor/liquid slug in a small range where the working fluid oscillates intermittently. When the power is raised to a medium value, the net force can overcome more flow resistance and the working fluid oscillates to and from in a much larger range. When the power is even higher, the net force easily surpasses the flow resistance, thereby generating a comparatively large flow inertia to complete flow cycles in a unitary direction.

Since PHP has no capillary limit, it is suitable for long distance heat transport or high-flux applications. Although PHP has no capillary limit, it has the issue of dry-out in horizontal or anti-gravity conditions due to its symmetrical structure; its performance relies heavily on the gravity-assistance. In fact, PHP with a few turns is not a functional subject to horizontal arrangements [1]. This is because the working fluid in the evaporation section cannot generate enough net force to overcome the flow resistance after evaporation, and the working fluid stops oscillating accordingly. Therefore, the lower temperature working fluid is unable to flow into the evaporation section, so that the temperature in the evaporation section rises rapidly. This state is called dry-out, and this had been clearly demonstrated in the PHP visualization experiment by Chien et al. [2].

The working fluid of PHP has a corresponding saturated vapor pressure in the evaporation section and the condensing section. Most of this vapor pressure usually cancels each other out, and the remaining net pressure difference is used to push the working fluid to move to and fro. Asymmetrical forces are generated by randomly distributed working fluid. When the force is sufficient to overcome the flow resistance of the working fluid, the working fluid starts to oscillate in a small range. This status is called startup, and there have been similar temperature curve of startup behaviors in the single loop pulsating heat pipe that is visualized by Khandekar and Groll [3].

PHPs are passive two-phase devices known for their manufacturing simplicity compared to other passive two-phase devices (i.e., conventional heat pipes). In order to prevent the bent pipes from collapsing on the outside and buckling inside the tube, it has a structural limitation in the radius of curvature. According to the standard JB/T5000.11 and Copper tube handbook [4], the limitation in the radius of curvature of copper tube is about 2.5–3 D_o. Such limitation causes huge heat spreading resistance between the heat spreading layer of the heating block or cooling block and PHP. Therefore, the amount of heat flux on the PHP is decreased appreciably.

To tackle the constraints of horizontal layout or inherited anti-gravity limitations, structural design is a common method, as shown in Table 1, in which the improvements in PHP can be divided into three parts, namely dual-diameter, external components, and 3D design. Chien et al. [2] and Yang et al. [5] conducted visual observation and heat transfer measurements for flat-plate pulsating heat pipes having a non-uniform channel configuration. Tseng et al. [6,7] has developed non-uniform cross section area PHPs and double pipe designs to facilitate unbalanced forces in horizontal and anti-gravity applications, respectively. Kwon and Kim [8] investigated the effect of a dual-diameter tube on the flow and heat transfer characteristics of single-turn pulsating heat pipes which were made of glass capillary tubes with various inner diameters.

Wan et al. [9] and Feng et al. [10] also designed the PHP to have a check valve integrated between two heating sections to create a one-way circulatory flow of working fluid. Taslimifar et al. [11] used the magnetic field in the evaporator and ferrofluid as PHP working fluid. Their results show that the thermal performance of an open loop PHP in both startup and steady state conditions was improved. Vries et al. [12] designed and tested the single turn PHP having a pair of Tesla-type valves, and successfully demonstrate a 14% decrease of thermal resistance. Pastukhov and Maydanik [13] studied the PHP having ball-valve or capillary barrier structures and showed that the presence of ball check valves reduced orientation sensitivity and thermal resistance while increased the maximum heating load by 10–14%. Torresin et al. [14] designed and tested a double condenser aluminum PHP; since the evaporating section is central, the thermal resistance of gravity-anti was same as the gravity-assist condition.

Mameli et al. [15] tested the startup characteristics in microgravity and proved that the operation is thermally induced using a hybrid loop thermosyphon/pulsating heat pipe. Deng et al. [16] studied the 3D-PHP, effects of number of turns, filling ratio and length of evaporating section and condensing section on the performance. Tseng et al. [17] studied the 3D-PHP and used a fin-and-tube heat exchanger as a condenser and found that the thermal module can handle a supplied power up to 1 kW and a maximum heat flux of 15.6 W/cm^2. Hathaway et al. [18] studied the Uneven-Turn 3D-PHP configuration to create an unbalanced force between the evaporating section and the condensing section, and successfully inverted the heat source.

From the forgoing literature survey, efforts stressed on resolving the problem of anti-gravity startup subject to high flux are still very rare. Hence, the objective of this study is to develop a three-dimensional configuration PHP having non-uniform cross section areas which is based on [2,6,16]. It is a ring-shaped structure containing non-uniform cross section areas, the ring-shaped portions are arranged in order alongside an axis so as to form the rectangle coiled having a compact arrangement structure which helps to prevent a high heat spreading resistance in the heating block and cooling block. Through this configuration, it can offer a much higher operating heat flux and the working fluid automatically flows along a specific direction due to unbalanced flow resistance and unbalanced capillary force between two adiabatic sections caused by non-uniform cross section areas of the adiabatic sections. It will be demonstrated shortly that the proposed non-uniform 3D-PHP is able to operate under anti-gravity situation, which is functional in high-flux applications.

Table 1. Main details of the previous studies in the literature.

Reference	Structure	Hydraulic Diameter (mm)	Working Fluid	Filling Ratio (%)	Input Power (W)
Chien et al. [2]	Dual-diameter	2 + 1.33	Water	40–70	10–100
Yang et al. [5]	Dual-diameter	0.27 + 0.33	Water Methanol	80	6–19
Tseng et al. [6]	Dual-diameter	2.4 + 1.31	Water Methanol HFE-7100	59.7 59.8 62.4	20–140
Tseng et al. [7]	Double-pipe	1.6 + 2.4	Methanol	50.1	40–220
Kwon and Kim [8]	Dual-diameter	1.2–2.2	Ethanol	50	5–25
Wan et al. [9]	Check valve	3	Water	70	100–500

Table 1. *Cont.*

Reference	Structure	Hydraulic Diameter (mm)	Working Fluid	Filling Ratio (%)	Input Power (W)
Feng et al. [10]	Check valve	3	Water	60	500
Taslimifar et al. [11]	Magnetic field	1.75	Ferrofluid	60	20
Vries et al. [12]	Tesla type valve	2	Water	50	10
Pastukhov and Maydanik [13]	Check valve	1.25	R-152a	40	10–40
Torresin et al. [14]	Double condenser	1.54	R245fa	40–75	500–2400
Mameli et al. [15]	3D-design	3	FC-72	50	18–182
Deng et al. [16]	3D-design	1.4	Methanol	50–80	95–578
Tseng et al. [17]	3D-design	3.4	Methanol	60	100–1000
Hathaway et al. [18]	Uneven-turn 3D-design	1.65	Water Acetone	65	50–400

2. Experiment Setup and Data Processing

The schematic of the non-uniform experimental apparatus is shown in Figure 2. The experimental setup consists of evaporator, condenser, water bath (YOTEC Instrument Corporation, Taiwan, model B20), direct current power supply, magnetic flowmeter, data acquisition module, and a non-uniform 3D-PHP. DC power supply contains a rated output voltage 60 V with accuracy of ±0.12 V; a rated output current 25 A with accuracy being ±0.075 A; and a maximum output power of 1500 W (Good Will Instrument Corporation, Taiwan, model PSU 60-25). A magnetic flowmeter with accuracy 0.35% and measurable range 0–12.8 L/min is used (Yokogawa Electric Corporation, Japan model AXF-005). Temperature acquisition module is used with a maximum measurement range of ±78 mV, sampling rate of 75 samples/s, and a 24-bit analog to digital converter (National Instrument Corporation, United States, model NI-9213). The evaporators were made of copper block (50 mm × 70 mm × 15 mm), and having six electronic heaters with a total equivalent resistance of 3 Ω. The condenser was made of copper block (50 mm × 70 mm × 15 mm) with volumetric flow rate of 1.25 L/min, and an inlet temperature of 50 °C. The objective of this study is to develop a passive solution for PHP upon high-flux applications. The test conditions mainly refer to the specifications from relevant manufacturers of next generation network switches. Note that the startup temperature is comparatively high, but it is not uncommon. In the meantime, the total input electric power is 811 W subject to an area of 67 mm × 67 mm, and the maximum temperature of system must be controlled below than 110 °C in an ambient temperature of 50 °C.
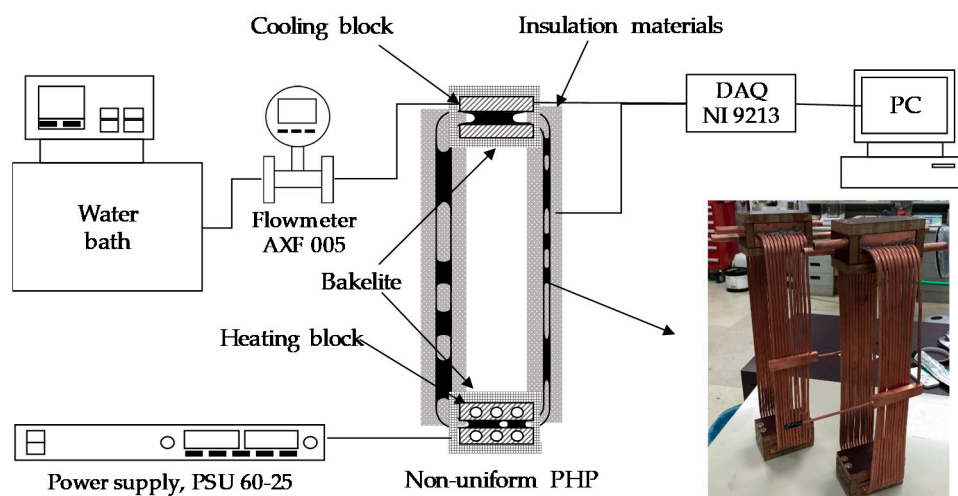

Figure 2. Experimental setup.

The conventional PHP has a structural limitation in the radius of curvature, and such a limitation causes the minimum distance between adjacent straight pipes to be about 2.5 D_o. For uniform area heat source, the heat spreading model can be simplified to the finite isotropic rectangular flux channel mode as shown in Figure 3. The heat-spreading resistance can be calculated by [19].

$$R_{\text{spreading}} = \frac{1}{k\pi^3\epsilon^2} \sum_{m=1}^{\infty} \frac{\sin^2(m\pi\epsilon)}{m^3} \left[\frac{m\pi + Bi\tanh(m\pi\tau)}{m\pi\tanh(m\pi\tau) + Bi} \right] \tag{1}$$

where relative contact area $\epsilon = a/c$, a is half the heating width, c is half the heat spreading width, relative layer thickness $\tau = t/c$, t is the heat-spreading thickness, Biot number $Bi = h/(ck)$, h is heat transfer coefficient, and k is the thermal conductivity of heat-spreading layer.
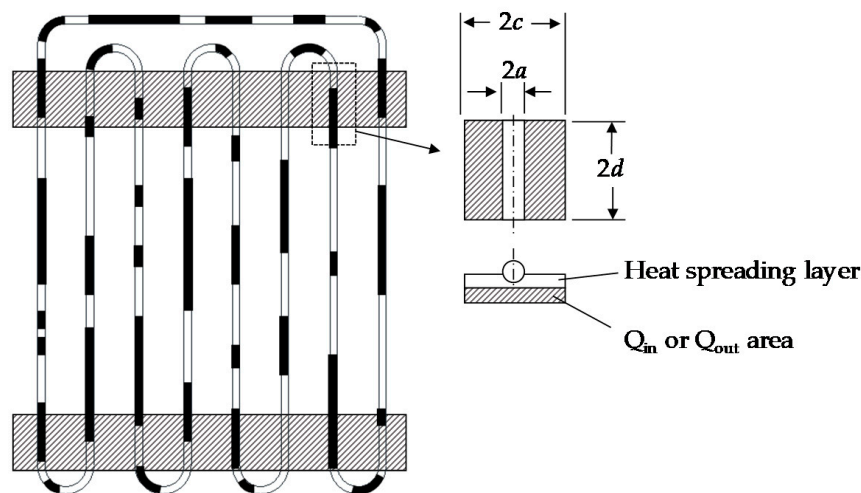

Figure 3. Schematic of simplified heat-spreading model.

This study proposes a compact arrangement PHP; the relative width ratio $\epsilon = a/c$ is close to 1, thus the heat spreading resistance is close to 0. Therefore, the compact arrangement PHP is suitable for a uniform area heat source, and the performance can be greater than a conventional PHP.

This assumes h = 5000 W/(m^{2}K), k = 400 W/(mK), $\tau = t/c = 0.333$, $\epsilon = a/c = 0.1$–1.0. The thermal resistance ratio can be calculated using Equation (1), and the results are shown in the Figure 4. The abscissa is relative ratio ϵ, which refers to the ratio of heat transport channel width to the total spreading width. The ordinate is relative thermal resistance ratio, which represents the ratio of spreading resistance to spreading resistance plus conduction resistance. For conventional PHPs, the relative width ratio $\epsilon \leq 0.4$, and the compact arrangement pulsating of this study can attain a value of $0.4 \leq \epsilon \leq 1$. The relative thermal resistance ratio of conventional PHP is 8.1% at $\epsilon = 0.4$. In this study, the relative ratio of the proposed PHP is $\epsilon = 0.857$ and relative thermal resistance ratio is only 0.6%, meaning a negligible influence of the spreading thermal resistance subject to the present compact arrangement of PHPs.

In this study, a ring-shaped rectangle PHP with non-uniform cross section areas was fabricated and tested, having an evaporating section, a condensing section, and two adiabatic sections, as shown in Figure 5.
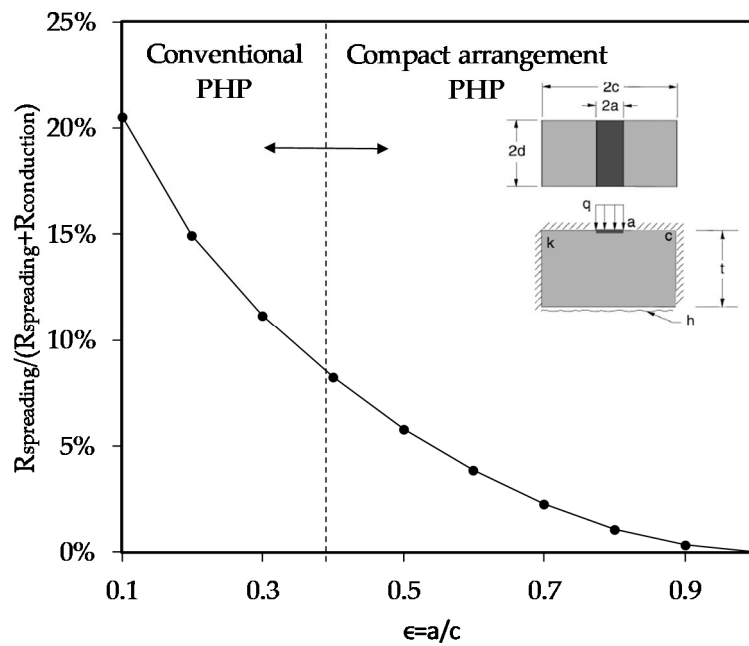
Figure 4. Relative heat spreading resistance percent for relative width ratio.
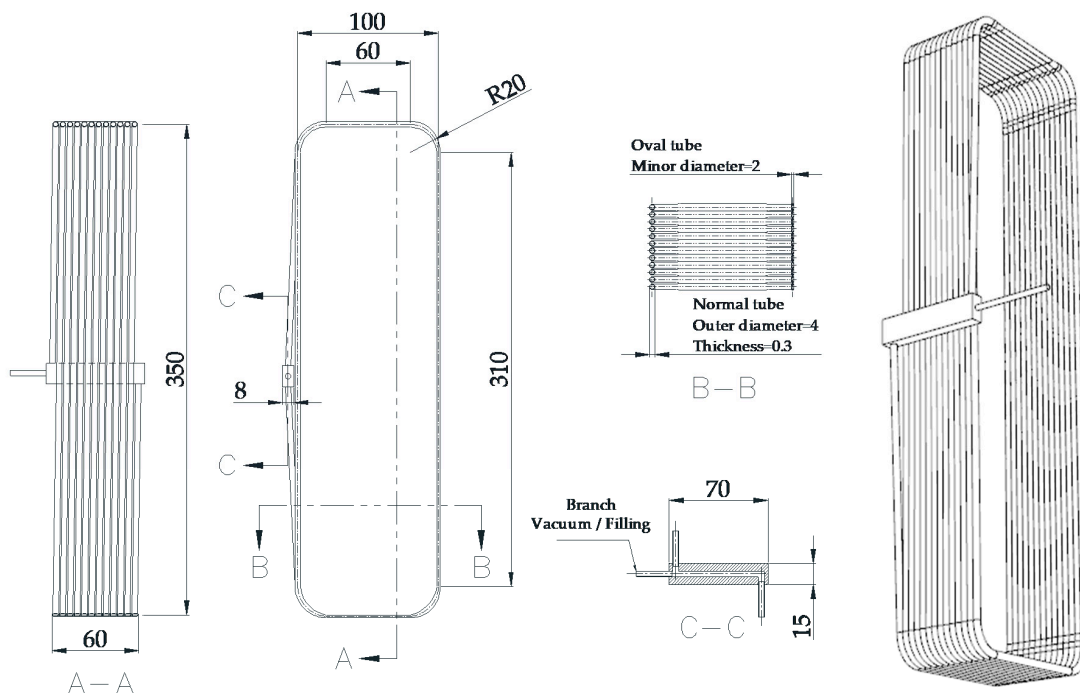

Figure 5. Schematic of the present pulsating heat pipe (Unit: mm).

For the present PHP, the outer diameter is 4.0 mm and the inner diameter is 3.4 mm. The heat transport distance between the evaporating section and condensing section is 350 mm, and the distance between two adiabatic sections is 100 mm. The PHP contains 12 turns with a radius of curvature of 20 mm. The tubes of the evaporating section and one side of the adiabatic section were compressed to form an oval configuration with a minor diameter being 2 mm and the hydraulic diameter $D_\mathrm{h} \approx 2.24$ mm, as shown in Figure 6. The total inner volume is about 95,876 mm^3, and methanol is used as the working fluid. Methanol has a lower evaporation temperature and a higher $\mathrm{d}P_\mathrm{sat}/\mathrm{d}T$ than water. The filling ratio (FR) is 38.7%.
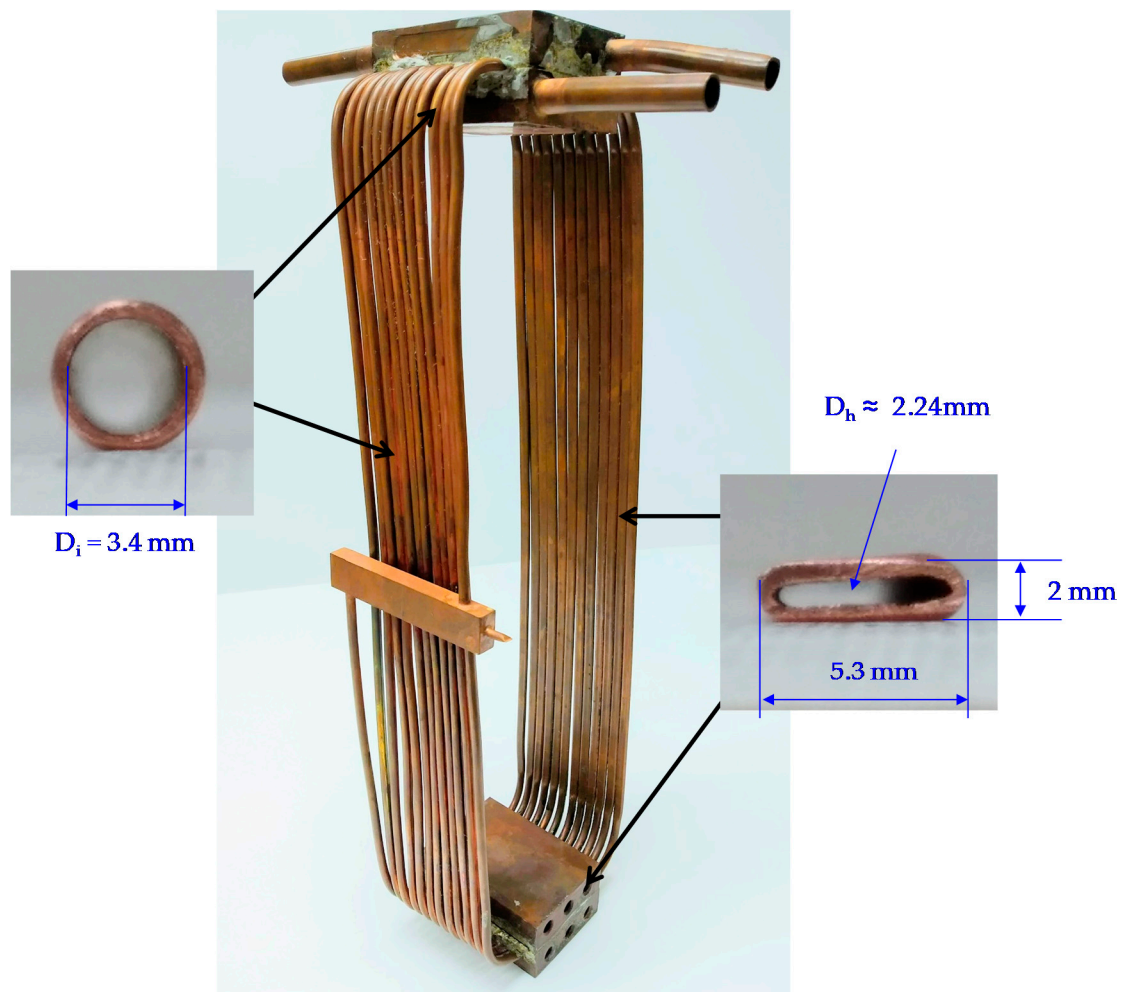
Figure 6. Photos of test PHP and cross sections.

The volumetric flowrate from thermostat water bath is 1.25 L/min with a supply temperature to maintain the cooling block at 50 °C. The DC power supply is used to regulate the heating power into the heating block ranging from 200 W to 800 W. The experiments were performed with gravity-assisted (bottom heating mode) and anti-gravity (top heating mode) conditions.

A total of 10 OMEGA T-type thermocouples were used, and the locations of the thermocouples and dimensions of the heating block and cooling block are shown in Figure 7. The lengths of the evaporating section and condensing section of the PHP are both 50 mm, respectively. Thermocouples were denoted as $T_{e,1}$–$T_{e,3}$ on heating block surface, $T_{c,1}$–$T_{c,3}$ on cooling block surface, $T_{ae,1}$–$T_{ae,2}$ on the adiabatic section tube surface 30 mm above the evaporating section, $T_{ac,1}$–$T_{ac,2}$ on the adiabatic section tube surface 30 mm above the condensing section. $T_{ae,1}$ and $T_{ac,1}$ were attached on the same tube of the circle side. $T_{ae,2}$ and $T_{ac,2}$ were attached on the same tube of the oval side. The sampling rate of the temperature signal recorder was set to 1.0 s.
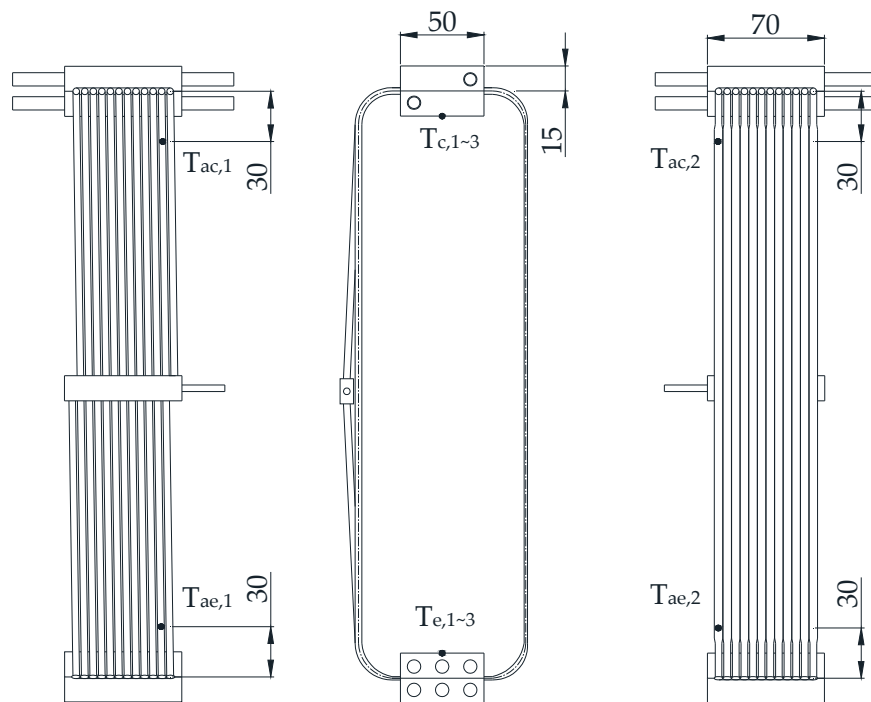
Figure 7. Dimensions of heating block and cooling block, and the locations of the thermocouples (Unit: mm).

The thermal resistance *R* of the present PHP was defined as temperature difference between the evaporating section and the condensing section divided by the input power, i.e.,:

$$R = \frac{T_{e,avg} - T_{c,avg}}{Q_{in}} \tag{2}$$

$$Q_{in} = V \times A \tag{3}$$

$$\overline{T_{i,j}} = \frac{1}{200} \sum_{t=1}^{200} (T_{i,j})_t \tag{4}$$

$$T_{e,avg} = \frac{\overline{T_{e,1}} + \overline{T_{e,2}} + \overline{T_{e,3}}}{3} \tag{5}$$

$$T_{c,avg} = \frac{\overline{T_{c,1}} + \overline{T_{c,2}} + \overline{T_{c,3}}}{3} \tag{6}$$

where subscript *t* of Equation (4) is the *t*-th second recorded value of temperature, $\overline{T_{i,j}}$ refers to the time-average temperature of the last 200 recorded value of temperature, $T_{e,avg}$ and $T_{c,avg}$ refers to position-average temperature of the heating block and cooling block, respectively.

The combined standard uncertainty in measurement of the thermal resistance can be referred from ISO/IEC GUM [20] and is calculated by following equation:

$$u_c^2(R) = \sum_{i=1}^{n} \left[\frac{\partial R}{\partial x_i} \right]^2 u^2(x_i) \tag{7}$$

where $u(x_i)$ and $\frac{\partial R}{\partial x_i}$ are standard uncertainties and the sensitivity coefficient of each measurement values, respectively.

Substituting Equations (2)–(6) into Equation (7) yields the combined standard uncertainty:

$$
\begin{aligned}
u_c^2(R) &= \left(\frac{\partial R}{\partial \overline{T_{e,1}}}\right)^2 u^2\left(\overline{T_{e,1}}\right) + \left(\frac{\partial R}{\partial \overline{T_{e,2}}}\right)^2 u^2\left(\overline{T_{e,2}}\right) + \left(\frac{\partial R}{\partial \overline{T_{e,3}}}\right)^2 u^2\left(\overline{T_{e,3}}\right) + \left(\frac{\partial R}{\partial \overline{T_{c,1}}}\right)^2 u^2\left(\overline{T_{c,1}}\right) \\
&\quad + \left(\frac{\partial R}{\partial \overline{T_{c,2}}}\right)^2 u^2\left(\overline{T_{c,2}}\right) + \left(\frac{\partial R}{\partial \overline{T_{c,3}}}\right)^2 u^2\left(\overline{T_{c,3}}\right) + \left(\frac{\partial R}{\partial V}\right)^2 u^2(V) + \left(\frac{\partial R}{\partial A}\right)^2 u^2(A)
\end{aligned}
\tag{8}
$$

The uncertainty of temperature measurement considered the following items, including the uncertainty inherited from the calibration standard, the rounding error in calculation, the accuracy of the data acquisition device, and the standard deviation of time-average temperature. The calibration standard used a platinum resistance thermometer. The third-party calibration standard was the Fluke Dry-Well Calibrator. The calibration range is 20 °C to 80 °C, step by 20 °C. The calibration contains an expanded uncertainty of 0.04 °C and a coverage factor of 2, and the uncertainty inherited from the calibration standard is:

$$
u_{\text{calibration standard}} = \frac{\text{expanded uncertainty}}{\text{coverage factor}}
\tag{9}
$$

The temperature data is rounded to one decimal place and the probability distribution was uniform distribution, the uncertainty of rounding error is:

$$
u_{\text{rounding}} = \frac{\text{minimum resolution}}{2\sqrt{3}}
\tag{10}
$$

According to the data acquisition device (National Instrument Corporation, United States, model NI-9213) datasheet, the resolution is ±38 μV and accuracy u_{DAQ} is ±0.77 °C.

The measurement standard deviation of time-average temperature is:

$$
u_{\text{measurement}} = \frac{S_{T_{i,j}}}{\sqrt{m}} = \frac{\sqrt{\frac{1}{m-1}\sum_{t=1}^{t=m}\left(\left(T_{i,j}\right)_t - \overline{T_{i,j}}\right)^2}}{\sqrt{m}}
\tag{11}
$$

The uncertainty of the temperature is:

$$
u^2\left(\overline{T_{i,j}}\right) = u_{\text{calibration standard}}^2 + u_{\text{rounding}}^2 + u_{\text{DAQ}}^2 + u_{\text{measurement}}^2
\tag{12}
$$

The uncertainty of power supply considered the rounding error and accuracy of instrument. The uncertainty of the power supply is:

$$
u^2(\text{power supply}) = u_{\text{rounding}}^2 + u_{\text{instrument}}^2
\tag{13}
$$

The uncertainties of each parameter are summarized in Table 2. For the gravity-assisted condition, under the input power of 200 W, 400 W, 600 W, and 800 W, the combined expanded uncertainties of the thermal resistance at a level of confidence of 95% are ±6.6%, ±3.5%, ±2.7%, and ±2.3%, respectively. For the anti-gravity condition, under the input power of 200 W, 400 W, 600 W, and 800 W, the combined expanded uncertainties of the thermal resistance at a level of confidence of 95% are ±3.8%, ±3.0%, ±2.6%, and ±2.3%, respectively.

Table 2. The uncertainties and sensitivity coefficient of parameters, Q_{in} = 200 W.

Parameters	Uncertainties
$u\left(\overline{T_{i,j}}\right)$	7.72×10^{-1}
$u(\text{V})$	1.52×10^{-2}
$u(\text{A})$	0.65×10^{-2}
$\frac{\partial R}{\partial T_{i,j}}$	1.65×10^{-3}
$\frac{\partial R}{\partial V}$	4.05×10^{-3}
$\frac{\partial R}{\partial A}$	1.23×10^{-2}
$U(Q_{in})$ *	$\pm 2.2\%$ or ± 4.5 W
$U(R)$ *	$\pm 6.6\%$ or ± 0.0066 K/W

* Coverage factor of 2, at a level of confidence of 95%.

3. Results and Discussion

An average temperature variation vs. elapsed time under gravity-assisted condition is shown in Figure 8. The experimental input power is increased from 200 W to 800 W with a step of 200 W, and the startup temperature of PHP at evaporator is about =80 °C ($T_{e,avg}$). Once the PHP is initiated, a pronounced drop of the $T_{e,avg}$ is encountered (about 10 °C). Subsequently, the steady state prevails at about $T_{e,avg}$ = 70 °C. On the other hand, the working fluid and the corresponding $T_{e,avg}$ oscillates with a small amplitude when the input power is less than 400 W. However, appreciable oscillations of the liquid/vapor slug occur to transport heat amid the evaporator and condenser when the input power rises to 600 W. Therefore, the fluctuations of $T_{e,avg}$ is comparatively large (~6 °C). A further rise of input power to 800 W result in an even pronounced oscillation frequency of the working fluid. However, then the fluctuation of the average temperature $T_{e,avg}$ is relatively small when compared to an input power of 600 W. This is because the thermal response falls behind the flow oscillation, thereby flow oscillation with higher frequency does not lead to appreciable temperature fluctuation.
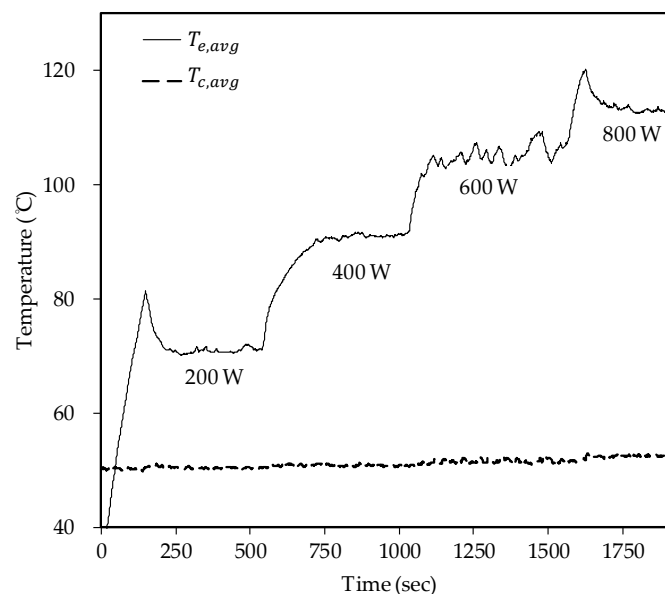

Figure 8. Average temperature variation vs. time for input power 200 W to 800 W; gravity-assisted condition (bottom heating mode).

An average temperature variation vs. elapsed time under anti-gravity condition is shown in Figure 9. The experiment input power is increased from 200 W to 800 W which is also in a step of 200 W. Note that the corresponding startup temperature ($T_{e,avg}$) is about = 90 °C while the steady state is reached at about $T_{e,avg}$ = 95 °C. When the input power is less than 400 W, the working fluid of the

PHP reveals a lower oscillation frequency, therefore the temperature oscillation can be clearly seen in Figure 9. Once the input power exceeds 600 W, the oscillation frequency of the working fluid also rises to yield a relatively stable $T_{e,\text{avg}}$.
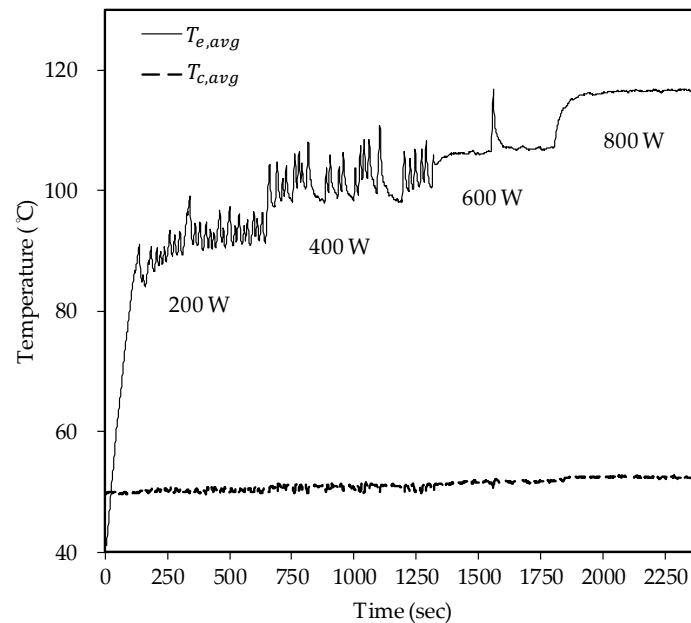

Figure 9. Average temperature variation vs. time for input power 200 W to 800 W; anti-gravity condition (top heating mode).

The temperature variation of the adiabatic section vs. time for input power 200 W to 800 W is shown in Figure 10. It can be observed that the temperature distributions are different. The left side of the charts show the gravity-assisted condition where the working fluid returns to the evaporator with the aid of gravity. Apparently, no appreciable temperature fluctuation is seen at a power of 200 W, but the oscillation frequency of temperature is increased with the rise of input power until Q = 600 W, and a further rise to 800 W leads to moderate fluctuation the temperature. The right side of the charts show the anti-gravity operation where the relative relationship of temperature distribution is similar for input power 200 W to 800 W, and the oscillation frequency of temperature increases as the input power increases. This is because the present PHP features an uneven inner diameter for the tubes in the adiabatic section. The circle side of the adiabatic section is D_i = 3.4 mm, which is slightly higher than the suggested upper limit $D_i \leq 2\sqrt{\sigma/(\rho_l - \rho_v)g} \approx 3.12$ mm (based on the properties of 80 °C) in the exiting literatures to activate PHP effectively. When the inner diameter of PHP is out of the recommend range, the flow pattern inside the tube can be referred to as the results of Khandekar and Groll [21]; the circle side of the adiabatic section is unable to sustain the flow-circulation, as shown in the Figure 11. In this regard, the working fluid returning to the evaporator can only be driven by capillary force and net pressure difference by the oval side, thereby forming a unitary circulation flow.
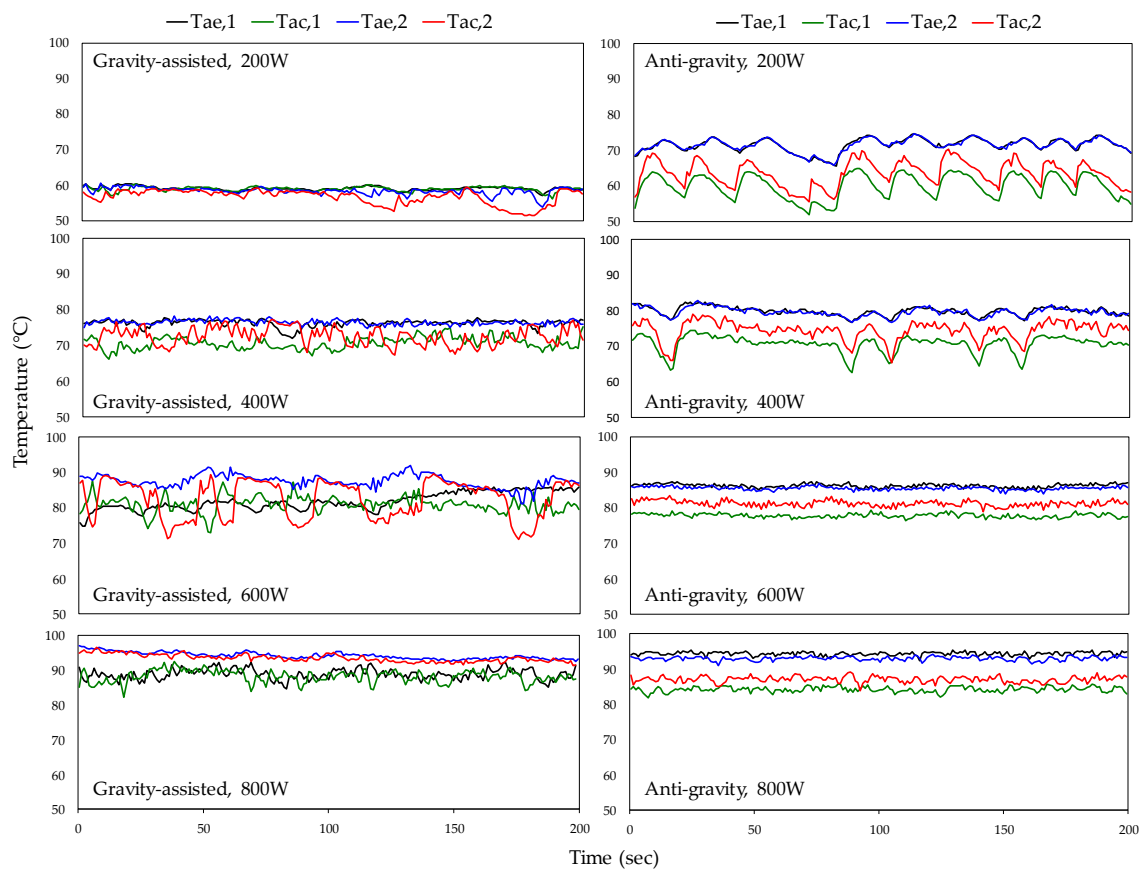
Figure 10. Adiabatic section temperature variation for proposed 3D-PHP.
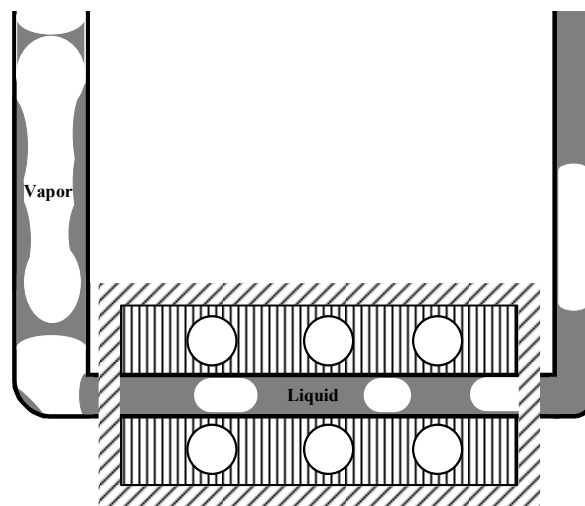

Figure 11. Dual diameter on the fluid distribution of PHP.

The corresponding average thermal resistance vs. input power is shown in Figure 12. When the input power is less than 400 W, the resultant force of the working fluid is insufficient to drive the working fluid stably, thereby yielding unstable oscillation. Hence, the thermal resistance of the anti-gravity condition is higher than that of the gravity-assisted operation. When input power is greater than 600 W, sufficient driving force is able to facilitate a stable oscillation to form a unitary circulation flow. In this regard, the difference in overall thermal resistance between gravity-assisted and anti-gravity operations is rather small. In fact, at an input power of 600 W, the thermal resistance of gravity-assisted and anti-gravity conditions is 0.0883 K/W and 0.0918 K/W, respectively. When the input

power is further raised to 800 W, the thermal resistance of gravity-assisted and anti-gravity conditions is 0.0761 K/W and 0.0796 K/W, respectively. In summary, the difference in thermal resistance between gravity-assisted and anti-gravity operations is less than 10% provided that a unitary circulation flow prevails. The results indicate that the proposed PHP is very suitable for high-flux applications where the inertial force of the working fluid may outweigh the influence of gravity.
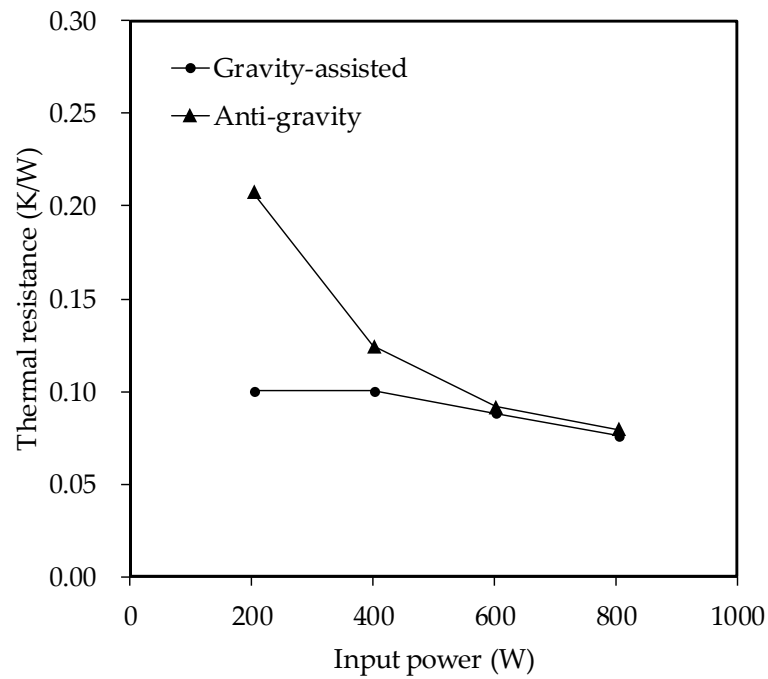

Figure 12. Thermal Resistance (K/W) vs. input power (W) of evaporator.

To further demonstrate the superiority of the proposed PHP, performance is in terms of thermal resistance ratio ($R_{\text{anti-gravity}}/R_{\text{gravity-assisted}}$) and supplied heat flux at the evaporator. The lower thermal resistance ratio indicates that PHP contains better capability to resist the negative influence caused by gravity. The associated performance index is used to compare the proposed PHP with existing literatures [7,9,10,16,18,22,23] is shown in Figure 13. Some further details amid the existing studies and the present one are listed in Table 3. As shown in the figure, the proposed PHP offers the highest heat flux of 22.9 W/cm^2 at a supplied power of 800 W while containing the least thermal resistance ratio ($R_{\text{anti-gravity}}/R_{\text{gravity-assisted}}$) of 1.05 when the input power is 800 W. Apparently, the proposed design is far better than the existing literatures [7,9,10,16,18,22,23], especially at a high supplied power like 600 W or 800 W, yet it still outperforms most of the existing studies even at a moderate power of 400 W.

For the typical PHP design, a small diameter tube is normally incorporated into the serpentine configuration to make use of the capillary force, yet bends formed in the condenser/evaporator sections normally require carefully mechanical machining to avoid severe deformations. In this regard, bends with large curvature are often used for serpentine PHPs. Unfortunately, this results in a decline in effective contact surface area between evaporator/condenser and PHP circuitry, thereby impairing the benefit of the wickless design of PHP. In essence, despite PHP offering a high-flux transporting characteristic, the thermal module incorporating PHPs normally fail to meet the high-flux demand. The present novel thermal module design offers a 3-D configuration which can cover higher contact surface area of PHP alongside the evaporator. The maximum heat transfer of the pulsating heat pipe is related to the total filling of the working fluid.

This study uses a compact arrangement design, meaning that at the same heat transfer distance more working fluid can be filled, so it contains a higher heat transfer than conventional design. When more working fluid is filled, the higher flow resistance in the pulsating heat pipe will be induced.

Therefore, optimal operating input power will increase accordingly and the thermal resistance at lower input power will also increase.
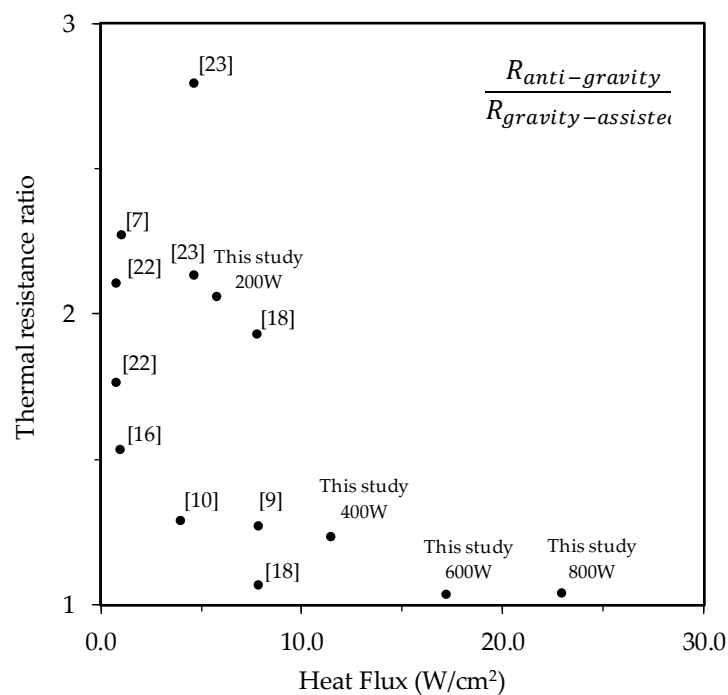

Figure 13. Thermal Resistance Ratio of anti-gravity condition to gravity-assisted condition vs. evaporating heat flux.

Table 3. Reference for comparison with this study and main parameters.

Reference	Working fluid, Filling Ratio	Q_{in} (W)	Evaporating Heat Flux (W/cm^2)	$\frac{R_{anti\text{-}gravity}}{R_{gravity\text{-}assisted}}$
Tseng et al. [7]	Methanol, 50%	160	1.0	2.28
Wan et al. [9]	Water, 70%	500	7.8	1.28
Feng et al. [10]	Water, 60%	500	3.9	1.29
Deng et al. [16]	Methanol, 70%	521	0.9	1.54
Hathaway et al. [18]	Water, 65%	398	7.8	1.93
Hathaway et al. [18]	Acetone, 65%	399	7.8	1.07
Riehl et al. [22]	Water, 70%	50	0.7	1.77
Riehl et al. [22]	Water-copper nanofluid, 70%	50	0.7	2.11
Vassilev et al. [23]	Water, 30%	400	4.6	2.14
Vassilev et al. [23]	Methanol, 30%	400	4.6	2.80
This study, 200 W	Methanol, 38%	200	5.7	2.06
This study, 400 W	Methanol, 38%	400	11.4	1.24
This study, 600 W	Methanol, 38%	600	17.1	1.04
This study, 800 W	Methanol, 38%	800	22.9	1.05

4. Conclusions

The present study proposed a novel high-flux PHP to ease the shortcomings of the conventional PHP, which is unable to function properly upon anti-gravity operations. The proposed PHP introduces additional unbalance force via uneven tube diameter/geometry in the adiabatic sections to tackle anti-gravity operation. The design contains a three-dimensional configuration circuitry with compact arrangement tubes on the evaporator and condenser to manage the high-power input situations. Through this design, the non-uniform 3D-PHP was fabricated and tested, and successfully tackled the anti-gravity with high-flux. The working fluid is methanol with 38% volumetric filling ratio. The input power ranges from 200 W to 800 W with a step of 200 W. For the gravity-assisted operation, the startup temperature of PHP at the evaporator is about =80 °C ($T_{e,avg}$). Once the PHP is activated, a

pronounced drop of the $T_{e,avg}$ is encountered (about 10 °C). Analogously, for anti-gravity operation, the corresponding startup temperature ($T_{e,avg}$) is slightly raised to about =90 °C while the steady state is reached at about $T_{e,avg}$ = 95 °C. The temperature fluctuation in the evaporator is first increased with the rise with heat flux but is moderately reduced at high-flux operations. By manipulating the uneven inner diameters of the adiabatic sections, the vapor tends to move to the lower frictional pressure drop side and the liquid tends to move to higher capillary force side, eventually forming a unitary flow that is able to withstand a much higher input power. The present PHP has a high-flux of 22.9 W/cm^2 and a low the thermal resistance ratio ($R_{anti-gravity}/R_{gravity-assisted}$) of 1.05 when the input power is 800 W. Both the heat flux and thermal resistance ratio are far better than existing literatures.

Author Contributions: Conceptualization, C.-Y.T.; Data curation, C.-Y.T.; Formal analysis, C.-Y.T. and K.-S.Y.; Investigation, C.-Y.T. and K.-S.Y.; Methodology, C.-Y.T. and K.-S.Y.; Project administration, C.-C.W.; Software, C.-Y.T.; Supervision, K.-S.Y. and C.-C.W.; Validation, K.-S.Y.; Writing—original draft, C.-Y.T.; Writing—review & editing, K.-S.Y. and C.-C.W. All authors have read and agreed to the published version of the manuscript.

Conflicts of Interest: The authors declare no conflict of interest.

Nomenclature

D_i	inner diameter, (mm)
D_o	outer diameter, (mm)
D_h	hydraulic diameter, (mm)
R	thermal resistance, (K/W)
Q_{in}	input power, (W)
T	temperature, (°C)
u_c	combined uncertainty
U	expanded uncertainty
S	standard deviation
x_i	estimate of input quantity
ρ_l	density of liquid, (kg/m^3)
ρ_v	density of vapor, (kg/m^3)
σ	surface tension, (N/m)
Bi	Biot number, hL/k
h	heat transfer coefficient, (W/(m^{2}K))
k	thermal conductivity, (W/(mK))
$\in$	relative contact size
τ	relative layer thickness
Subscript	
avg	average
c	condenser
e	evaporator
ae	adiabatic tube near evaporator
ac	adiabatic tube near condenser

References

1. Charoensawan, P.; Terdtoon, P. Thermal performance of horizontal closed-loop oscillating heat pipes. *Appl. Therm. Eng.* **2008**, *28*, 460–466. [CrossRef]
2. Chien, K.-H.; Lin, Y.-T.; Chen, Y.-R.; Yang, K.-S.; Wang, C.-C. A novel design of pulsating heat pipe with fewer turns applicable to all orientations. *Int. J. Heat Mass Transf.* **2012**, *55*, 5722–5728. [CrossRef]
3. Khandekar, S.; Groll, M. An insight into thermo-hydrodynamic coupling in closed loop pulsating heat pipes. *Int. J. Therm. Sci.* **2004**, *43*, 13–20. [CrossRef]

4. Copper Development Association Inc. *The Copper Tube Handbook*; Copper Development Association Publication: New York, NY, USA, 2010.

5. Yang, K.-S.; Cheng, Y.-C.; Liu, M.-C.; Shyu, J.-C. Micro pulsating heat pipes with alternate microchannel widths. *Appl. Therm. Eng.* **2015**, *83*, 131–138. [CrossRef]

6. Tseng, C.-Y.; Yang, K.-S.; Chien, K.-H.; Jeng, M.-S.; Wang, C.-C. Investigation of the performance of pulsating heat pipe subject to uniform/alternating tube diameters. *Exp. Therm. Fluid Sci.* **2014**, *54*, 85–92. [CrossRef]

7. Tseng, C.-Y.; Yang, K.-S.; Chien, K.-H.; Wu, S.-K.; Wang, C.-C. A novel double pipe pulsating heat pipe design to tackle inverted heat source arrangement. *Appl. Therm. Eng.* **2016**, *106*, 697–701. [CrossRef]

8. Kwon, G.H.; Kim, S.J. Operational characteristics of pulsating heat pipes with a dual-diameter tube. *Int. J. Heat Mass Transf.* **2014**, *75*, 184–195. [CrossRef]

9. Wan, Z.; Wang, X.; Feng, C. Heat transfer performances of the capillary loop pulsating heat pipes with spring-loaded check valve. *Appl. Therm. Eng.* **2020**, *167*, 114803. [CrossRef]

10. Feng, C.; Wan, Z.; Mo, H.; Tang, H.; Lu, L.; Tang, Y. Heat transfer characteristics of a novel closed-loop pulsating heat pipe with a check valve. *Appl. Therm. Eng.* **2018**, *141*, 558–564. [CrossRef]

11. Taslimifar, M.; Mohammadi, M.; Afshin, H.; Saidi, M.H.; Shafii, M.B. Overall thermal performance of ferrofluidic open loop pulsating heat pipes: An experimental approach. *Int. J. Therm. Sci.* **2013**, *65*, 234–241. [CrossRef]

12. De Vries, S.F.; Florea, D.; Homburg, F.G.A.; Frijns, A.J.H. Design and operation of a Tesla-type valve for pulsating heat pipes. *Int. J. Heat Mass Transf.* **2017**, *105*, 1–11. [CrossRef]

13. Pastukhov, V.G.; Maydanik, Y.F. Development of a pulsating heat pipe with a directional circulation of a working fluid. *Appl. Therm. Eng.* **2016**, *109*, 155–161. [CrossRef]

14. Torresin, D.; Agostini, F.; Mularczyk, A.; Agostini, B.; Habert, M. Double condenser pulsating heat pipe cooler. *Appl. Therm. Eng.* **2017**, *126*, 1051–1057. [CrossRef]

15. Mameli, M.; Catarsi, A.; Mangini, D.; Pietrasanta, L.; Michè, N.; Marengo, M.; Di Marco, P.; Filippeschi, S. Start-up in microgravity and local thermodynamic states of a hybrid loop thermosyphon/pulsating heat pipe. *Appl. Therm. Eng.* **2019**, *158*, 113771. [CrossRef]

16. Deng, Z.; Zheng, Y.; Liu, X.; Zhu, B.; Chen, Y. Experimental study on thermal performance of an anti-gravity pulsating heat pipe and its application on heat recovery utilization. *Appl. Therm. Eng.* **2017**, *125*, 1368–1378. [CrossRef]

17. Tseng, C.-Y.; Wu, H.-M.; Wong, S.-C.; Yang, K.-S.; Wang, C.-C. A Novel Thermal Module with 3-D Configuration Pulsating Heat Pipe for High-Flux Applications. *Energies* **2018**, *11*, 3425. [CrossRef]

18. Hathaway, A.A.; Wilson, C.A.; Ma, H.B. Experimental Investigation of Uneven-Turn Water and Acetone Oscillating Heat Pipes. *J. Thermophys. Heat Transf.* **2012**, *26*, 115–122. [CrossRef]

19. Yovanovich, M.; Muzychka, Y.; Culham, J. Spreading resistance of isoflux rectangles and strips on compound flux channels. *J. Thermophys. Heat Transf.* **1999**, *13*, 495–500. [CrossRef]

20. International Organization for Standardization. *Uncertainty of Measurement-Part 3: Guide to the Expression of Uncertainty in Measurement*; ISO/IEC 98-3; ISO: Geneva, Switzerland, 2008.

21. Khandekar, S.; Groll, M. On the definition of pulsating heat pipes: An overview. In Proceedings of the 5th Minsk International Seminar (Heat Pipes, Heat Pumps and Refrigerators), Minsk, Belarus, 8–11 September 2003; pp. 707–719.

22. Riehl, R.R.; dos Santos, N. Water-copper nanofluid application in an open loop pulsating heat pipe. *Appl. Therm. Eng.* **2012**, *42*, 6–10. [CrossRef]

23. Vassilev, M.; Avenas, Y.; Schaeffer, C.; Schanen, J.-L.; Schulz-Harder, J. Experimental study of a pulsating heat pipe with combined circular and square section channels. In Proceedings of the 2007 IEEE Industry Applications Annual Meeting, New Orleans, LA, USA, 23–27 September 2007; pp. 1419–1425.